

Dijet Angular Distributions from $\bar{p}p$ Collisions at $\sqrt{s} = 1.8$ TeV

F. Abe,⁽¹⁶⁾ D. Amidei,⁽³⁾ G. Apollinari,⁽¹¹⁾ G. Ascoli,⁽⁷⁾ M. Atac,⁽⁴⁾ P. Auchincloss,⁽¹⁴⁾ A. R. Baden,⁽⁶⁾ A. Barbaro-Galtieri,⁽⁹⁾ V. E. Barnes,⁽¹²⁾ F. Bedeschi,⁽¹¹⁾ S. Behrends,⁽¹²⁾ S. Belforte,⁽¹¹⁾ G. Bellettini,⁽¹¹⁾ J. Bellinger,⁽¹⁷⁾ J. Bensinger,⁽²⁾ A. Beretvas,⁽¹⁴⁾ P. Berge,⁽⁴⁾ S. Bertolucci,⁽⁵⁾ S. Bhadra,⁽⁷⁾ M. Binkley,⁽⁴⁾ R. Blair,⁽¹⁾ C. Blocker,⁽²⁾ J. Bofill,⁽⁴⁾ A. W. Booth,⁽⁴⁾ G. Brandenburg,⁽⁶⁾ D. Brown,⁽⁶⁾ A. Byon,⁽¹²⁾ K. L. Byrum,⁽¹⁷⁾ M. Campbell,⁽³⁾ R. Carey,⁽⁶⁾ W. Carithers,⁽⁹⁾ D. Carlsmith,⁽¹⁷⁾ J. T. Carroll,⁽⁴⁾ R. Cashmore,⁽⁴⁾ F. Cervelli,⁽¹¹⁾ K. Chadwick,^(4,12) T. Chapin,⁽¹³⁾ G. Chiarelli,⁽¹¹⁾ W. Chinowsky,⁽⁹⁾ S. Cihangir,⁽¹⁵⁾ D. Cline,⁽¹⁷⁾ D. Connor,⁽¹⁰⁾ M. Contreras,⁽²⁾ J. Cooper,⁽⁴⁾ M. Cordelli,⁽⁵⁾ M. Curatolo,⁽⁵⁾ C. Day,⁽⁴⁾ R. DelFabbro,⁽¹¹⁾ M. Dell'Orso,⁽¹¹⁾ L. DeMortier,⁽²⁾ T. Devlin,⁽¹⁴⁾ D. DiBitonto,⁽¹⁵⁾ R. Diebold,⁽¹⁾ F. Dittus,⁽⁴⁾ A. DiVirgilio,⁽¹¹⁾ J. E. Elias,⁽⁴⁾ R. Ely,⁽⁹⁾ S. Errede,⁽⁷⁾ B. Esposito,⁽⁵⁾ B. Flaughner,⁽¹⁴⁾ E. Focardi,⁽¹¹⁾ G. W. Foster,⁽⁴⁾ M. Franklin,^(6,7) J. Freeman,⁽⁴⁾ H. Frisch,⁽³⁾ Y. Fukui,⁽⁸⁾ A. F. Garfinkel,⁽¹²⁾ P. Giannetti,⁽¹¹⁾ N. Giokaris,⁽¹³⁾ P. Giromini,⁽⁵⁾ L. Gladney,⁽¹⁰⁾ M. Gold,⁽⁹⁾ K. Goulios,⁽¹³⁾ C. Grosso-Pilcher,⁽³⁾ C. Haber,⁽⁹⁾ S. R. Hahn,⁽¹⁰⁾ R. Handler,⁽¹⁷⁾ R. M. Harris,⁽⁴⁾ J. Hauser,⁽³⁾ T. Hessing,⁽¹⁵⁾ R. Hollebeck,⁽¹⁰⁾ P. Hu,⁽¹⁴⁾ B. Hubbard,⁽⁹⁾ P. Hurst,⁽⁷⁾ J. Huth,⁽⁴⁾ H. Jensen,⁽⁴⁾ R. P. Johnson,⁽⁴⁾ U. Joshi,⁽¹⁴⁾ R. W. Kadel,⁽⁴⁾ T. Kamon,⁽¹⁵⁾ S. Kanda,⁽¹⁶⁾ D. A. Kardelis,⁽⁷⁾ I. Karliner,⁽⁷⁾ E. Kearns,⁽⁶⁾ R. Kephart,⁽⁴⁾ P. Kesten,⁽²⁾ H. Keutelian,⁽⁷⁾ S. Kim,⁽¹⁶⁾ L. Kirsch,⁽¹⁰⁾ K. Kondo,⁽¹⁶⁾ U. Kruse,⁽⁷⁾ S. E. Kuhlmann,⁽¹²⁾ A. T. Laasanen,⁽¹²⁾ W. Li,⁽¹⁾ T. Liss,⁽³⁾ N. Lockyer,⁽¹⁵⁾ F. Marchetto,⁽¹⁵⁾ R. Markeloff,⁽¹⁷⁾ L. A. Markosky,⁽¹⁷⁾ P. McIntyre,⁽¹⁵⁾ A. Menzione,⁽¹¹⁾ T. Meyer,⁽¹⁵⁾ S. Mikamo,⁽⁸⁾ M. Miller,⁽¹⁰⁾ T. Mimashi,⁽¹⁶⁾ S. Miscetti,⁽⁵⁾ M. Mishina,⁽⁸⁾ S. Miyashita,⁽¹⁶⁾ N. Mondal,⁽¹⁷⁾ S. Mori,⁽¹⁶⁾ Y. Morita,⁽¹⁶⁾ A. Mukherjee,⁽⁴⁾ C. Newman-Holmes,⁽⁴⁾ L. Nodulman,⁽¹⁾ R. Paoletti,⁽¹¹⁾ A. Para,⁽⁴⁾ J. Patrick,⁽⁴⁾ T. J. Phillips,⁽⁶⁾ H. Piekarz,⁽²⁾ R. Plunkett,⁽¹³⁾ L. Pondrom,⁽¹⁷⁾ J. Proudfoot,⁽¹⁾ G. Punzi,⁽¹¹⁾ D. Quarrie,⁽⁴⁾ K. Ragan,⁽¹⁰⁾ G. Redlinger,⁽³⁾ J. Rhoades,⁽¹⁷⁾ F. Rimondi,⁽⁴⁾ L. Ristori,⁽¹¹⁾ T. Rohaly,⁽¹⁰⁾ A. Roodman,⁽³⁾ A. Sansoni,⁽⁵⁾ R. Sard,⁽⁷⁾ V. Scarpine,⁽⁷⁾ P. Schlabach,⁽⁷⁾ E. E. Schmidt,⁽⁴⁾ P. Schoessow,⁽¹⁾ M. H. Schub,⁽¹²⁾ R. Schwitters,⁽⁶⁾ A. Scribano,⁽¹¹⁾ S. Segler,⁽⁹⁾ M. Sekiguchi,⁽¹⁶⁾ P. Sestini,⁽¹¹⁾ M. Shapiro,⁽⁶⁾ M. Sheaff,⁽¹⁷⁾ M. Shibata,⁽¹⁶⁾ M. Shochet,⁽³⁾ J. Siegrist,⁽⁹⁾ P. Sinervo,⁽¹⁰⁾ J. Skarha,⁽¹⁷⁾ D. A. Smith,⁽⁷⁾ F. D. Snider,⁽³⁾ R. St.Denis,⁽⁶⁾ A. Stefanini,⁽¹¹⁾ Y. Takaiwa,⁽¹⁶⁾ K. Takikawa,⁽¹⁶⁾ S. Tarem,⁽²⁾ D. Theriot,⁽⁴⁾ A. Tollestrup,⁽⁴⁾ G. Tonelli,⁽¹¹⁾ Y. Tsay,⁽³⁾ F. Ukegawa,⁽¹⁶⁾ D. Underwood,⁽¹⁾ R. Vidal,⁽⁴⁾ R. G. Wagner,⁽¹⁾ R. L. Wagner,⁽⁴⁾ J. Walsh,⁽¹⁰⁾ T. Watts,⁽¹⁴⁾ R. Webb,⁽¹⁵⁾ T. Westhusing,⁽⁷⁾ S. White,⁽¹³⁾ A. Wicklund,⁽¹⁾ H. H. Williams,⁽¹⁰⁾ T. Yamanouchi,⁽⁴⁾ A. Yamashita,⁽¹⁶⁾ K. Yasuoka,⁽¹⁶⁾ G. P. Yeh,⁽⁴⁾ J. Yoh,⁽⁴⁾ and F. Zetti⁽¹¹⁾

⁽¹⁾Argonne National Laboratory, Argonne, Illinois 60439

⁽²⁾Brandeis University, Waltham, Massachusetts 02254

⁽³⁾University of Chicago, Chicago, Illinois 60637

⁽⁴⁾Fermi National Accelerator Laboratory, Batavia, Illinois 60510

⁽⁵⁾Laboratori Nazionali di Frascati, Istituto Nazionale di Fisica Nucleare, Frascati, Italy

⁽⁶⁾Harvard University, Cambridge, Massachusetts 02138

⁽⁷⁾University of Illinois, Urbana, Illinois 61801

⁽⁸⁾National Laboratory for High Energy Physics (KEK), Tsukuba-gun, Ibaraki-ken 305, Japan

⁽⁹⁾Lawrence Berkeley Laboratory, Berkeley, California 94720

⁽¹⁰⁾University of Pennsylvania, Philadelphia, Pennsylvania 19104

⁽¹¹⁾Istituto Nazionale di Fisica Nucleare, University and Scuola Normale Superiore of Pisa, Pisa, Italy

⁽¹²⁾Purdue University, West Lafayette, Indiana 47907

⁽¹³⁾Rockefeller University, New York, New York 10021

⁽¹⁴⁾Rutgers University, Piscataway, New Jersey 08854

⁽¹⁵⁾Texas A&M University, College Station, Texas 77843

⁽¹⁶⁾University of Tsukuba, Ibaraki 305, Japan

⁽¹⁷⁾University of Wisconsin, Madison, Wisconsin 53706

(Received 24 March 1989)

We have measured dijet angular distributions at $\sqrt{s} = 1.8$ TeV with the Collider Detector at Fermilab and the Tevatron $\bar{p}p$ Collider and find agreement with leading-order QCD. By comparing the distribution for the highest dijet invariant masses with the prediction of a model of quark compositeness, we set a lower limit on the associated scale parameter Λ_c at 330 GeV (95% C.L.).

PACS numbers: 13.87.-a, 12.38.Qk 12.50.Ch, 13.85.Ni

We have used the Collider Detector at Fermilab (CDF) and the Fermilab Tevatron to measure dijet angular distributions in $\bar{p}p$ collisions at $\sqrt{s} = 1.8$ TeV, complementing our measurement of the single-jet inclusive cross section.¹ The measured angular distributions are compared to leading-order QCD predictions for various parton momentum distribution functions, and the data are used to investigate the presence of possible quark-compositeness effects.

The CDF has been described in detail elsewhere.² This analysis uses data from the electromagnetic and hadronic calorimeters and the vertex time-projection chambers. The calorimeters are divided into three regions of pseudorapidity ($\eta = -\ln \tan \theta/2$): central ($|\eta| \leq 1.1$), plug ($1.1 \leq |\eta| \leq 2.4$), and forward ($2.4 \leq |\eta| \leq 4.2$). The central calorimeter consists of lead-scintillator and iron-scintillator sandwiches arranged in projective towers with a segmentation of $\Delta\eta \times \Delta\phi = 0.1 \times 15^\circ$. The absolute energy scale for single particles interacting in the central calorimeter has been determined in a test beam to 2% accuracy, and the calibration was maintained at a 3% level using radioactive sources, light pulsers, and electronic charge injection systems.³ The plug and forward calorimeters consist of lead and iron planes instrumented in layers with gas proportional chambers. Cathode-pad readout of these calorimeters form projective towers with a segmentation of $\Delta\eta \times \Delta\phi = 0.1 \times 5^\circ$. The gas calorimeters were used in this analysis to determine the position of jets. The time-projection chambers are used to determine the position of the event vertex along the beam line.

The trigger consisted of (a) coincidence of at least one particle in each of the scintillator hodoscopes ($3.24 \leq |\eta| \leq 5.90$) located on opposite sides of the interaction region; (b) total transverse energy in the calorimeters above 20, 30, 40, or 45 GeV, depending on the instantaneous luminosity. The corresponding integrated luminosities for data collected at each threshold are 0.4, 14.9, 6.3, and 7.2 nb^{-1} . The total transverse energy was calculated by summing the transverse electromagnetic energy and the central hadronic transverse energies above 1 GeV in a uniform trigger tower segmentation of $\Delta\eta \times \Delta\phi = 0.2 \times 15^\circ$. The transverse energy in a tower is defined as $E \sin \theta$, where E is the energy in the tower and θ is the tower polar angle.

In the off-line analysis spurious triggers from accelerator losses and cosmic rays were removed using timing information in the central hadron calorimeter. Large pulses in the gas calorimeters characterized by large energy deposition in a single tower and chamber, believed to be due to neutron interactions,⁴ were removed on an event by event basis.

Jets are identified as local clusters of energy in the calorimeter by a clustering algorithm,¹ which uses a cone size of $(\Delta\eta^2 + \Delta\phi^2)^{1/2} = 1.0$ (where ϕ is in rad) to optimize jet energy resolution. A four-vector is associated with each cluster, and the jet transverse momentum (p_t)

is defined by treating the energy in each calorimeter cell within the cone as corresponding to that of a massless particle.

Each event was required to have a *trigger jet* with $p_t \geq 45$ GeV/c in the central detector. In order to insure that the cluster energy was well contained within the central calorimeter, the axis of its centroid was required to be no closer than 0.2 units of pseudorapidity to the central-plug calorimeter boundary. A second jet was required to be within $|\eta| \leq 4.2$ and in the hemisphere opposite the trigger jet in azimuth. The above selection resulted in a sample of 5943 events.

The trigger-jet requirement of $p_t \geq 45$ GeV/c was 98% efficient for all four total-transverse-energy hardware thresholds. This efficiency was determined from data taken at the low thresholds of 20 and 30 GeV, where it was found that only 2% of the events containing a jet with $p_t \geq 45$ GeV/c had less than 45 GeV of total transverse energy in the trigger hardware of the central detector.

The pseudorapidities of the trigger and second jet were used to define $\eta^* = (\eta_1 - \eta_2)/2$ for the jet axis in the dijet center of mass, and the average pseudorapidity, $\eta_{\text{boost}} = (\eta_1 + \eta_2)/2$. The scattering angle θ^* is related to η^* by $\tanh \eta^* = \cos \theta^*$. The invariant mass of the dijet system is taken to be $M_{jj} = p_t' \cosh \eta^*$, where p_t' is the parton momentum corresponding to the trigger-jet p_t , after corrections for detector response and jet fragmentation.⁵

The restrictions on the pseudorapidities of the two jets and the minimum transverse momentum of the trigger jet correspond to coupled constraints on the center-of-mass variables M_{jj} , η_{boost} , and $\cos \theta^*$. Measuring large values of $\cos \theta^*$ requires large values of M_{jj} and larger geometric acceptance corrections.⁶ The data were analyzed separately in three (overlapping) samples: $|\eta^*|$

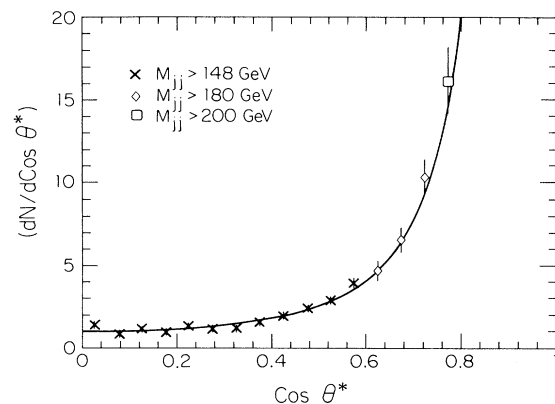


FIG. 1. Dijet angular distribution for the combined data sample: $M_{jj} \geq 148$ GeV/c², $M_{jj} \geq 180$ GeV/c², and $M_{jj} \geq 200$ GeV/c². In all cases, $|\eta_{\text{boost}}| \leq 1.2$. The curve shown is the QCD prediction discussed in text. Statistical and systematic uncertainties are combined.

$\leq 0.7, 1.0$, and 1.2 , necessitating corresponding cuts of $M_{jj} > 148, 180$, and $200 \text{ GeV}/c^2$. Acceptance corrections for each sample account for geometric effects, nonzero dijet transverse momentum, and calorimeter energy resolution. These corrections have been calculated using ISAJET and a calorimeter simulation.⁷ The calorimeter resolution and the effect of additional jets were determined by examining the distributions of components of the dijet transverse momentum.⁸ The relative

acceptance corrections are dominated by the pseudorapidity requirement on the trigger jet, vary slowly with $\cos\theta^*$, and do not exceed $\pm 30\%$ for any of the three angular intervals analyzed. A small systematic error (5%) in acceptance arises from uncertainties in the transverse momentum of the dijet system.

The lowest-order QCD prediction of the cross section for $\bar{p}p \rightarrow \text{jet } 1 + \text{jet } 2 + X$ may be written in terms of three orthogonal parton center-of-mass variables $\cos\theta^*$, η_{boost} , and M_{jj} as the following:⁹

$$\frac{d\sigma}{d\eta_{\text{boost}} dM_{jj} d\cos\theta^*} = \left(\frac{\pi\alpha_s^2(Q^2)}{32E_{\text{beam}}^4} \right) (2M_{jj}) \sum_{12} \left(\frac{F(x_1, Q^2)}{x_1} \right) \left(\frac{F(x_2, Q^2)}{x_2} \right) |M_{12}|^2, \quad (1)$$

where $\alpha_s(Q^2)$ is the strong coupling strength, E_{beam} is the energy of the proton beam, $|M_{12}|$ is the parton scattering matrix element, x_1 (x_2) is the fraction of the proton (antiproton) momentum carried by the parton, and $F(x_1, Q^2)$ is the parton momentum distribution. The momentum transfer is specified by Q^2 . The t -channel exchange of gluons dominates the behavior of the matrix element and predicts a distribution similar to the Rutherford cross section, $dN/d\cos\theta^* \sim \sin^{-4}\theta^*/2$. When expressed in terms of $\chi \equiv (1 + \cos\theta^*)/(1 - \cos\theta^*)$, the leading-order QCD prediction is approximately constant for large χ .

The acceptance-corrected $dN/d\cos\theta^*$ distribution for the combined data set is shown in Fig. 1. Data from the two higher-mass intervals are normalized to the low-mass data sample in the angular region of overlap ($\cos\theta^* \leq 0.6$). The QCD prediction (curve) calculated for a sum over gluons and four quark flavors, agrees well with the data over the entire mass interval, although the dominant contribution to the sum in Eq. (1) changes from gluon-gluon to quark-gluon scattering as the dijet invariant mass increases. We find a negligible variation of the prediction with different structure-function choices¹⁰ or process scales Q^2 , within the range $4p_t^2$ to

$p_t^2/4$. Combining statistical and systematic errors in quadrature, we obtain a fit with a χ^2/N_{DF} of 16/15; separate fits to the three constituent-mass intervals give similar agreement.

Our data can be used to test for the possible presence of a contact interaction between quarks. We modified the matrix element M_{12} to include a contact interaction of the type suggested by Eichten, Lane, and Peskin,¹¹ with a characteristic energy scale Λ_c . This choice leads to the largest effect in the high-mass data sample where quark-antiquark scattering gives a larger contribution. Fits to the highest-mass distribution of $dN/d\chi$ are shown in Fig. 2. After accounting for uncertainties in the parton distribution functions and a 7% systematic error in the parton energy scale, we find a lower limit on Λ_c of 330 GeV at 95% confidence level ($\chi^2/N_{\text{DF}} = 17/9$). This limit is lower than the previously published value of $\Lambda_c \geq 700 \text{ GeV}$ obtained from our single-jet inclusive spectrum,¹ but is determined here by an independent method. Our result may be compared directly with the limit of $\Lambda_c \geq 415 \text{ GeV}$ set by the UA1 Collaboration¹² using a similar method and a larger integrated luminosity at $\sqrt{s} = 630 \text{ GeV}$.

The authors wish to thank the CDF technical-support staff for their help throughout the course of assembling and commissioning the detector. We are also indebted to the staff of the Tevatron Collider for their work in the first physics run. This work was supported by the Department of Energy, the National Science Foundation, Istituto Nazionale di Fisica Nucleare, Italy, the Ministry of Science, Culture and Education of Japan, and the A. P. Sloan Foundation.

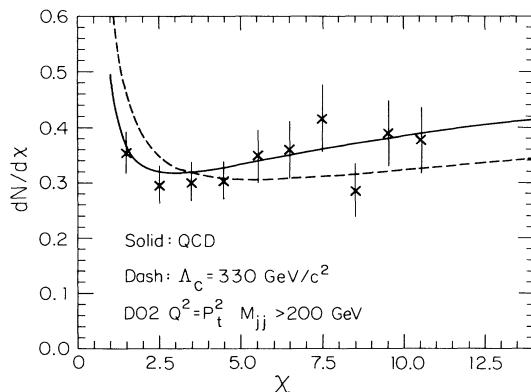


FIG. 2. Compositeness limit derived from the χ distribution for $M_{jj} \geq 200 \text{ GeV}/c^2$. The curves are QCD ($\Lambda_c = \infty$) and the composite model ($\Lambda_c = 330 \text{ GeV}$), which is excluded by the data with 95% confidence limit.

¹CDF Collaboration, F. Abe *et al.*, Phys. Rev. Lett. **62**, 613 (1989); also S. Kuhlmann, Ph.D. thesis, Purdue University, 1988 (unpublished); and CDF Collaboration, A. Garfinkel, in *Proceedings of Seventh Topical Workshop on Proton-Antiproton Collider Physics*, edited by R. Raja and J. Yoh (Fermilab, Batavia, 1988).

²F. Abe *et al.*, Nucl. Instrum. Methods Phys. Res., Sect. A **271**, 387 (1988).

³L. Balka *et al.*, Nucl. Instrum. Methods Phys. Res., Sect. A **276**, 272 (1988); S. Bertolucci *et al.*, Nucl. Instrum. Methods Phys. Res., Sect. A **267**, 301 (1988).

⁴CDF Collaboration, M. Franklin, in *Proceedings of Seventh Topical Workshop on Proton-Antiproton Collider Physics*, edited by R. Raja and J. Yoh (Fermilab, Batavia, 1988).

⁵The correction was determined using the ISAJET Monte Carlo event generator (version 5.38) with parameters selected to reproduce CDF jet-fragmentation data and a detector simulation based on measured response of the calorimeters to single particles. For example, a 45-GeV cluster in the central detector corresponds to a 60-GeV parton. ISAJET is described in F. Paige and S. Protopopescu, in *Proceedings of the Summer Study on the Physics of the Superconducting Supercollider, Snowmass, Colorado, 1986*, edited by R. Donaldson and J. Marx (Division of Particles and Fields of the American Physical Society, New York, 1986), p. 320. The CDF jet-fragmentation data are described in B. Hubbard, in Ref. 4.

⁶R. St. Denis, Ph.D. thesis, Harvard University, 1988 (unpublished); Argonne National Laboratory Report No. ANL-HEP-TR-89-02 (unpublished).

⁷C. Newman-Holmes and J. Freeman, in *Proceedings of the Workshop on Detector Simulation for the SSC*, Argonne, IL, 1987, edited by L. E. Price (Argonne National Laboratory Report No. ANL-HEP-CP-80-51), pp. 190, 285. This simulation bends charged particles in the magnetic field and uses measured single-particle response to deposit energy in the calorimeter. Since this publication the simulator geometry has been made realistic, uninstrumented regions response tuned to test beam data, and gas calorimeter response improved.

⁸We have followed the technique outlined in P. Babnaia *et al.*, Phys. Lett. **144B**, 283 (1984).

⁹R. K. Ellis and J. Sexton, Nucl. Phys. **B269**, 445 (1986). Calculations are based on the code supplied to us by R. K. Ellis and M. Mangano.

¹⁰E. Eichten *et al.*, Rev. Mod. Phys. **56**, 579 (1984); D. W. Duke and J. F. Owens, Phys. Rev. D **30**, 49 (1984).

¹¹The Lagrangian of the contact interaction is taken to be the product of two left-handed color-singlet and isosinglet currents: cf. E. Eichten, K. Lane, and M. Peskin, Phys. Rev. Lett. **50**, 811 (1983).

¹²G. Arnison *et al.*, Phys. Lett. B **177**, 244 (1986).